International Journal of Solids and Structures 73–74 (2015) 55–66

Contents lists available at ScienceDirect

International Journal of Solids and Structures

journal homepage: www.elsevier.com/locate/ijsolstr

Wave propagation in equivalent continuums representing truss lattice materials

Mark C. Messner *, Matthew I. Barham, Mukul Kumar, Nathan R. Barton

Lawrence Livermore National Laboratory, P.O. Box 808, L-227, Livermore, CA 94551, USA

ARTICLE INFO

Article history:
Received 22 March 2015
Received in revised form 15 May 2015
Available online 29 July 2015

Keywords:
Meta-materials
Micro-mechanics
Additive manufacturing
Wave propagation
Trusses

ABSTRACT

Stiffness scales linearly with density in stretch-dominated lattice meta-materials offering the possibility of very light yet very stiff structures. Current additive manufacturing techniques can assemble structures from lattice materials, but the design of such structures will require accurate, efficient simulation methods. Equivalent continuum models have several advantages over discrete truss models of stretch dominated lattices, including computational efficiency and ease of model construction. However, the development an equivalent model suitable for representing the dynamic response of a periodic truss in the small deformation regime is complicated by microinertial effects. This paper derives a dynamic equivalent continuum model for periodic truss structures suitable for representing long-wavelength wave propagation and verifies it against the full Bloch wave theory and detailed finite element simulations. The model must incorporate microinertial effects to accurately reproduce long wavelength characteristics of the response such as anisotropic elastic soundspeeds. The formulation presented here also improves upon previous work by preserving equilibrium at truss joints for simple lattices and by improving numerical stability by eliminating vertices in the effective yield surface.

1. Introduction

The development of additive manufacturing (AM) techniques allows the design of both the macroscale and microscale geometry of a structural component (Kruth et al., 1998; Murr et al., Jan. 2012; Rosen, 2007). Control over the micro-geometry opens up a new design space, effectively allowing the designer to control the properties of a material by varying the material's structure. Lattice materials are a promising class of micro-geometries, offering excellent stiffness-to-weight ratios and simple construction by tiling the periodic unit cell into a macroscale shape (Evans et al., 2001; Warren and Kraynik, 1987). A subclass of lattice materials are stretch dominated lattice materials, where the principal deformation mechanism is axial deformation of the struts. Because the scaling between stiffness and density in these structures is linear they offer the possibility of exceptionally light but stiff materials (Zheng et al., 2014).

The classic structure where deformation occurs through axial stretching and compression of a series of connected struts is the truss. Stretch dominated lattice materials then resemble periodic trusses, albeit on a smaller length scale than typical structural trusses (Hutchinson and Fleck, 2006; Martinsson and Babuška, 2007). Experimental and computational studies of discrete truss structures reveal complicated dynamic behavior, including the existence of band gaps (Howard and Pao, 1998; Signorelli and von Flotow, 1988) and microjetting under impact loading (Winter et al., 2014). Representing these complex phenomena with an equivalent continuum model is challenging. An equivalent continuum model is a material formulation which replaces a periodic discrete structure with a continuum that deforms equivalently. Equivalent continuum models have several advantages over discrete simulations: they integrate more easily into existing finite element frameworks; they generally reduce the computational complexity, measured in number of degrees of freedom, required to represent a periodic structure; and they eliminate the difficulty inherent in meshing a complex microgeometry.

This work fills a gap in previous research on modeling periodic truss systems by focusing on the wave propagation properties of equivalent continuums. Previous research by Pao et al. (1999), Srikantha Phani et al. (2006) and Yong and Lin (1992) describes models of discrete trusses under dynamic loading. Hutchinson and Fleck (2006) and Mohr (2005) develop equivalent continuum models of trusses under quasi-static loading, which are discussed in more detail subsequently. However, no work to date formulates an equivalent continuum model suitable for representing wave

* Corresponding author. Tel.: +1 925 423 1540.
E-mail address: messner6@llnl.gov (M.C. Messner).

http://dx.doi.org/10.1016/j.ijsolstr.2015.07.023
0020-7683/

propagation in periodic truss structures. Such a model must consider the inertial properties of periodic trusses in addition to elastic and plastic properties. Microinertial effects accounting for the actual mechanism of wave propagation through the discrete microstructure become significant when the material is loaded dynamically (Fish et al., 2002b,a; Fish et al., 2012; Wang and Sun, 2002). Typically, a model incorporates microinertial effects in order to better represent the dispersion of higher order deformation modes. This work demonstrates that a model must consider microinertial effects to accurately represent the long wavelength response of a periodic truss, even though the long wavelength limit only exercises the lowest deformation modes. The equivalent continuum model described here improves upon previous models by developing a formula for the resolved tension in the truss members that better preserves equilibrium at the joints. The formulation also eliminates numerical instabilities in the plastic flow rule via a method gleaned from an analogy to crystal plasticity models.

The presentation of the model is organized as follows. Section 2 describes previous equivalent continuum models by Hutchinson and Fleck (2006) and Mohr (2005) and describes the problem of vertices on the effective yield surface. Section 3 derives an equivalent continuum model for periodic truss structures, including long wavelength microinertial effects. Section 4 verifies the model against quasi-static and dynamic finite element simulations of a discrete octet truss and the Bloch wave theory. Finally, Section 5 summarizes the work and describes possible future uses of the model.

2. Quasi-static elastic and plastic equivalent continuum models

A truss is a structural system comprised of joints connected by members called struts. The mechanical assumption of the system is that the joints are structural pins that do not transfer moment and, correspondingly, that the struts transmit only axial forces. In a periodic truss, the combination of a motif and lattice describes the position of all joints. A motif is a collection of vectors describing the position of joints about a common point. Hutchinson and Fleck (2006) refer to each vector as a joint basis vector and the collection of vectors as the joint basis. A lattice is a set of vectors describing the translational symmetry of these common points. The linear combination

$$\mathbf{x}_i = \sum_{k=1}^{n} m_k \mathbf{b}_k \tag{1}$$

describes the position of any lattice point i in a lattice for the set of lattice vectors $\mathbf{b}_k$ and any set of integers m_k. Here n is the dimensionality of the system. Similarly, the position or, equivalently, the connectivity of the struts must also have translational symmetry described by the lattice vectors. Hutchinson and Fleck (2006) describe the position of the struts with a set of vectors called the strut basis. An infinite, periodic truss does not consider boundary effects – the lattice extends to infinity in all directions. A single unit cell, encompassing all the symmetries of the periodic truss, fully describes such a structure. Fig. 1 shows one possible unit cell for a periodic octet-truss.

Hutchinson and Fleck (2006) describe a method based on the Bloch wave theory for calculating the effective equivalent elastic tensor for any 2D or 3D periodic truss structure. Their approach is to calculate the sum of the strain energy in all struts in the unit cell for an arbitrary macrostrain field, divide by the unit cell volume to find the strain energy density, and then take the second derivative with respect to the strain to find the effective elastic stiffness tensor. The strain energy density per unit reference volume in an arbitrary, linear elastic truss with constant Young's moduli is given by

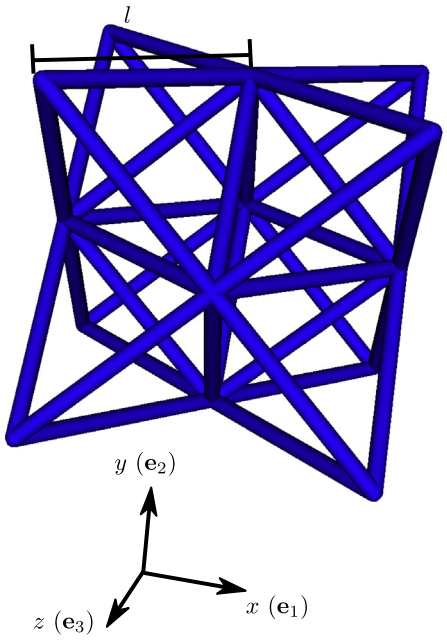

Fig. 1. Octet truss unit cell. All struts have equal lengths l. The three lattice vectors have the same length and point in the directions of the indicated cartesian coordinate system. Therefore, for this unit cell the octet truss is a simple cubic lattice.

$$\Phi(\boldsymbol{\varepsilon}) = \frac{E}{2V_0} \sum_{i=1}^{n_{struts}} A_i l_i \varepsilon_i^2 \tag{2}$$

where V_0 is the reference unit cell volume, E is the Young's modulus, A_i the strut cross-sectional area, l_i the strut length, and ε_i the axial strain of a strut under a given loading. Assuming the deformation remains affine for all joints, the strain in each strut is

$$\varepsilon_i = \mathbf{n}_i \cdot \boldsymbol{\varepsilon} \cdot \mathbf{n}_i \tag{3}$$

where $\boldsymbol{\varepsilon}$ is the macroscale strain tensor and $\mathbf{n}_i$ the strut normal. Taking the second derivative with respect to strain yields the formula

$$\mathbf{C} = E\bar{\rho}\hat{\mathbf{C}} \tag{4}$$

with

$$\hat{\mathbf{C}} = \frac{\sum_{s=1}^{n_{struts}} A_i l_i \mathbf{n}_i \otimes \mathbf{n}_i \otimes \mathbf{n}_i \otimes \mathbf{n}_i}{\sum_{i=1}^{n_{struts}} l_i A_i}. \tag{5}$$

Here $\bar{\rho}$ is the relative density of the equivalent continuum – the ratio of the density of the truss as a whole to the density of the solid material comprising the struts – assuming the volume of the joints is small. This formula and that of Hutchinson and Fleck (2006) produce the same equivalent elasticity tensor for simple lattices – periodic trusses for which a Bravais lattice alone with no motif describes the position of the joints.

Mohr (2005) describes a theory of equivalent continuum plasticity for truss structures. The theory first defines yield criteria for individual struts, for example plastic yielding and elastic buckling. Mohr then defines the yield surface of the equivalent continuum material to be the locus of points in stress space that cause any single strut to yield. Fig. 2 shows a 2D slice in stress space of the yield surface this method generates for the octet truss, only considering a single yield state of σ_0 in either compression or tension. In the full stress space these types of yield surfaces consist of the intersection of hyperplanes, with one hyperplane for each yield criteria in each strut. Associated plastic flow then occurs in

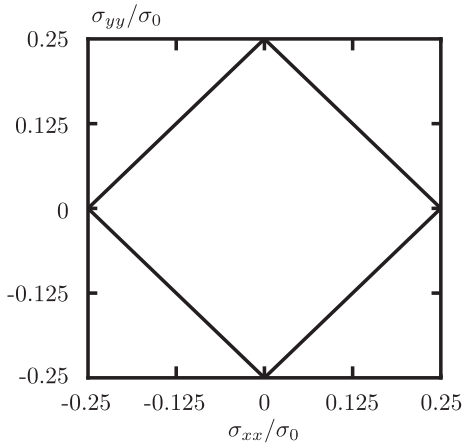

Fig. 2. The yield surface of the octet truss for $\bar{\rho} = 0.9$, defined as the locus of strut yield stresses, projected onto the σ_{xx}–σ_{yy} plane.

directions normal to the yield surface. The problem with this definition of equivalent plasticity is the vertices where multiple hyperplanes intersect. At these points, there is no clearly defined normal to the yield surface and plastic flow becomes degenerate. This causes numerical instability in the implemented plasticity model – a problem which has also been observed in models of plasticity for rate-independent single crystals (Kocks, 1998). The equivalent continuum model developed in this work solves this problem of vertices and also introduces a correction to Mohr's formula for the tension resolved in each strut.

3. Plastic deformation

3.1. Pressure sensitive, viscoplastic flow

Consider the unit cell of a periodic truss structure. Starting with elasticity, given the displacements of the joints a and b defining strut i, the elongation of the strut is

$$e_i = \mathbf{n}_i \cdot (\mathbf{d}_a - \mathbf{d}_b) \tag{6}$$

with $\mathbf{n}_i$ the strut normal, $\mathbf{n}_i = (\mathbf{x}_a - \mathbf{x}_b)/l_i$ for $\mathbf{x_a}$ and $\mathbf{x_b}$ the nodal positions and $l_i = \|\mathbf{x}_a - \mathbf{x}_b\|$, and $\mathbf{d}_a$ and $\mathbf{d}_b$ the displacements of joints a and b, respectively. Assuming a linear relation between engineering strain and stress, the stress in the strut is

$$\sigma_i = \frac{E}{l_i}\mathbf{n}_i \cdot (\mathbf{d}_a - \mathbf{d}_b) \tag{7}$$

with E the Young's modulus of the struts. Assume the Cauchy-Born hypothesis with a simple lattice. Then the displacement of any joint in the periodic truss under an applied macroscopic strain field $\boldsymbol{\varepsilon}(\mathbf{x})$ is affine and given by

$$\mathbf{d}_a = \boldsymbol{\varepsilon} \cdot \mathbf{x}_a. \tag{8}$$

Now consider plasticity. Additively decompose the strain into elastic and plastic parts $\boldsymbol{\varepsilon} = \boldsymbol{\varepsilon}^e + \boldsymbol{\varepsilon}^p$. Eq. (8) becomes

$$\mathbf{d}_a = (\boldsymbol{\varepsilon}^e + \boldsymbol{\varepsilon}^p) \cdot \mathbf{x}_a = \mathbf{d}_a^e + \mathbf{d}_a^p \tag{9}$$

with $\mathbf{d}_a^e := \boldsymbol{\varepsilon}^e \cdot \mathbf{x}_a$ and $\mathbf{d}_a^p := \boldsymbol{\varepsilon}^p \cdot \mathbf{x}_a$. Assume that only elastic strut displacements cause stress in Eq. (7). Section 2 shows, based on Hutchinson and Fleck (2006), that the relation between stress and elastic strain for any periodic truss comprised of struts with the same elastic stiffness, but possibly different areas, is

$$\boldsymbol{\sigma} = \bar{\rho} E \hat{\mathbf{C}} : \boldsymbol{\varepsilon}^e \tag{10}$$

where $\hat{\mathbf{C}}$ is a unitless second order tensor which depends on the strut lengths and areas and the truss topology. Inverting Eq. (10) and combining with Eqs. (7) and (8) yields a formula relating macroscale stress to the strut tension:

$$\sigma_i = \frac{1}{\bar{\rho}}\mathbf{n}_i \cdot \hat{\mathbf{C}}^{-1} : \boldsymbol{\sigma} \cdot \frac{\mathbf{x}_a - \mathbf{x}_b}{l_i} \tag{11}$$

Recognizing that $\mathbf{n}_i = \frac{\mathbf{x}_a - \mathbf{x}_b}{l_i}$ and rearranging the equation yields:

$$\sigma_i = \frac{1}{\bar{\rho}}(\mathbf{n}_i \otimes \mathbf{n}_i) : \hat{\mathbf{C}}^{-1} : \boldsymbol{\sigma} \tag{12}$$

Note the strong similarity of this equation to Eq. (13) of Mohr (2005):

$$\sigma_i = \frac{1}{c_i}\boldsymbol{\sigma} : (\mathbf{n}_i \otimes \mathbf{n}_i) \tag{13}$$

with c_i the volume fraction of the strut. See Fig. 3 for examples of the different load distributions generated for an octet truss by these two different strut tension expressions. Consider the indicated joint for the uniaxial load case. Three struts meet at this joint with strut normals $\mathbf{n}_1 = [\sqrt{2}/2 \quad 0 \quad \sqrt{2}/2]$, $\mathbf{n}_2 = [0 \quad \sqrt{2}/2 \quad \sqrt{2}/2]$, and $\mathbf{n}_3 = [\sqrt{2}/2 \quad \sqrt{2}/2 \quad 0]$ with respect to the coordinate system shown in the figure. Periodicity reduces the force from the adjacent unit cells to direction $\mathbf{n}_4 = [1 \quad 0 \quad 0]$. As the figure shows, calculating the strut tensions via Eq. (13) and determining the resulting nodal equilibrium equation yields

$$\mathbf{0} = f_1\mathbf{n}_1 + 0\mathbf{n}_2 + f_3\mathbf{n}_3 + f_4\mathbf{n}_4. \tag{14}$$

Summing forces in the y-direction shows that this joint cannot be in equilibrium. However, Eq. (12) correctly generates a compressive force in the strut with normal $\mathbf{n}_2$, satisfying the nodal equilibrium condition. This is a general feature of Eq. (12), provided the lattice topology is simple, because the stress state assumed by Eqs. (4) and (5) minimizes the internal energy. In contrast, complex lattices require explicitly solving for the equilibrium joint positions and strut forces.

Eq. (12) also resembles the expression for calculating the shear resolved along a single system in a crystal plasticity model (see, for example Asaro, 1983). Section 2 described the yield surface of periodic trusses and observed the degeneracy of plastic flow at yield surface vertices. Models of grain-scale plasticity in metals, for example the Taylor–Bishop–Hill theory of rate-independent, faced-centered cubic, single crystal plasticity encounter the same problem (Bishop and Hill, 1951b,a). The solution typically adopted by crystal plasticity models is to make the yield surface moderately rate-sensitive (Kocks, 1998). Adopting this approach for periodic trusses smooths the yield surface at the intersection of the hyperplanes representing strut limit states (see Fig. 2), preventing degenerate flow at the vertices. Plastic flow in actual materials is at least somewhat rate sensitive, so at the worst introducing a moderate rate sensitivity into the model simply overestimates the physical rate sensitivity.

There is a fundamental similarity between crystal plasticity models and equivalent truss models – both seek to describe the deformation of lattice materials. In crystal models the material consists of individual atoms positioned in a lattice. For a truss model, the lattice consists of the joints. The key differences between the two types of models is the deformation mechanism under consideration – for crystals shear along crystallographic planes; for trusses axial deformation along the struts. Nevertheless, the final systems of equations of the two models are very similar.

For small deformations, the elastic tensor relates the rate of elastic strain to the stress rate:

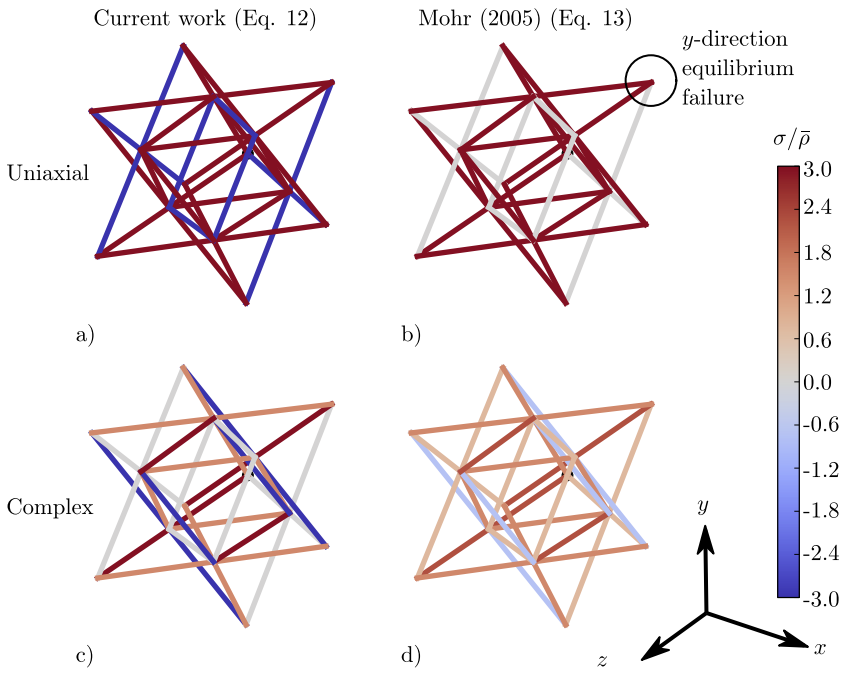

Fig. 3. Strut tensions from the two different strut tension formulas (Eq. (12) from this work and Eq. (13) from Mohr (2005)) for an octet truss under two different stress states. State "Uniaxial" is uniaxial, x-direction tension ($[\sigma \quad 0 \quad 0 \quad 0 \quad 0 \quad 0]$) and state "Complex" is a combination of biaxial x–y tension and xz shear ($[\sigma/4 \quad \sigma/4 \quad 0 \quad 0 \quad \sigma/4 \quad 0]$). The formula from Mohr (2005) develops non-equilibrium strut tensions, as demonstrated for the y-direction of the indicated joint for the uniaxial loading.

$$\dot{\boldsymbol{\sigma}} = \bar{\rho} E \hat{\mathbf{C}} : (\dot{\boldsymbol{\varepsilon}} - \dot{\boldsymbol{\varepsilon}}^p). \tag{15}$$

Following the ideas of crystal plasticity kinematics, the plastic strain rate is assumed to be an additive composition of uniaxial strains along each strut in the truss unit cell:

$$\dot{\boldsymbol{\varepsilon}}^p = \sum_{i=1}^{n_{struts}} \dot{\varepsilon}_i (\mathbf{n}_i \otimes \mathbf{n}_i). \tag{16}$$

The uniaxial strain rate along each strut varies with the tensile stress in the strut via a power law, rate dependent formula:

$$\dot{\varepsilon}_i = \dot{\varepsilon}_0 \left| \frac{\sigma_i}{\bar{\sigma}_i} \right|^{n-1} \frac{\sigma_i}{\bar{\sigma}_i} \tag{17}$$

where σ_i is the strut stress, defined by Eq. (12), $\bar{\sigma}_i$ the uniaxial strut flow stress, $\dot{\varepsilon}_0$ a reference strain rate, and n the rate-sensitivity parameter. This expression is essentially identical to the resolved shear/slip equation commonly adopted for crystal plasticity models (see, for example, Roters et al. (2010)) but replaces shear stress and strain with tensile stress and strain. Let $\dot{\varepsilon}_0 = \sqrt{2/3 \dot{\boldsymbol{\varepsilon}} : \dot{\boldsymbol{\varepsilon}}}$, the effective strain rate, and use $n = 20$ for low-to-moderate rate sensitivity.

In general the model can track the flow stress separately in each strut. This requires maintaining a history variable for each strut. To reduce the computational expense of tracking and updating these variables the formulation adopts, again from crystal plasticity, the idea of isotropic hardening:

$$\dot{\bar{\sigma}}_i = \dot{\bar{\sigma}} = H \sum_{i=1}^{n_{struts}} |\dot{\varepsilon}_i| \tag{18}$$

$$\bar{\sigma}(t = 0) = \sigma_0$$

where σ_0 is the yield stress of the struts and H the hardening modulus.

While these expressions are for small deformations, the similarity of Eqs. (12), (15)–(18) to their crystal plasticity counterparts implies methods of extending crystal plasticity kinematics to large deformations apply equally well to the periodic truss equations, provided the deformation remains affine. For example, methods of computing and applying the large rotations for crystal plasticity (e.g. Hill and Rice, 1972; Forest and Pilvin, 1999; Messner et al., 2015) also apply to the periodic truss. Even the interpretation of these rotations is similar between the two models: in crystal plasticity large rotations represent the deformation of the atomic lattice, in the periodic truss model they represent the deformation of the lattice of truss joints. This analogy breaks down with the presence of internal degrees of freedom (complex lattices). In this case, the updated joint positions would require explicit consideration of internal equilibrium. The updated joint coordinates, including rotations, could be calculated by minimizing the strain energy as a function of the position of the internal degrees of freedom.

A coupled, implicit integration of Eqs. (15) and (18) supplemented by Eqs. (12), (16) and (18) define the model. Algorithm 1 summarizes the stress update procedure. In the algorithm, Eq. (12) defines the strut tensions σ_i. The appendix details the Jacobian function required in the material update.

Algorithm 1. Stress update procedure for the periodic truss model

function UPDATE($\Delta\boldsymbol{\varepsilon}_{n+1}, \boldsymbol{\sigma}_n, \bar{\sigma}_n$)
  $\mathbf{x} \leftarrow [\boldsymbol{\sigma}_n \quad \bar{\sigma}_n]$
  $\Delta\varepsilon_0 \leftarrow \sqrt{2/3 \Delta\boldsymbol{\varepsilon}_{n+1} : \Delta\boldsymbol{\varepsilon}_{n+1}}$
  while $\|\mathbf{R}\| > tol$ **do**
    $\Delta\boldsymbol{\varepsilon}^p \leftarrow \sum_{i=1}^{n_{struts}} \Delta\varepsilon_0 \left|\frac{\sigma_i}{\bar{\sigma}}\right|^{n-1} \frac{\sigma_i}{\bar{\sigma}} (\mathbf{n}_i \otimes \mathbf{n}_i)$
    $\mathbf{R}_\sigma \leftarrow (1 + \mathrm{tr}\Delta\boldsymbol{\varepsilon}^p)\boldsymbol{\sigma} - \boldsymbol{\sigma}_n - \bar{\rho} E \hat{\mathbf{C}} \cdot (\Delta\boldsymbol{\varepsilon}_{n+1} - \Delta\boldsymbol{\varepsilon}^p)$
    $R_{\bar{\sigma}} \leftarrow \bar{\sigma} - \bar{\sigma}_n - H \sum_{i=1}^{n_{struts}} \Delta\varepsilon_0 \left|\frac{\sigma_i}{\bar{\sigma}}\right|^n$
    $\mathbf{R} \leftarrow [\mathbf{R}_\sigma \quad R_{\bar{\sigma}}]$
    $\mathbf{J} \leftarrow$ JACOBIAN $(\boldsymbol{\sigma}, \bar{\sigma}, \Delta\boldsymbol{\varepsilon}_{n+1})$
    $\Delta\mathbf{x} \leftarrow -\mathbf{J}^{-1} \cdot \mathbf{R}$
    $\mathbf{x} \leftarrow \mathbf{x} + \Delta\mathbf{x}$
    $[\boldsymbol{\sigma} \quad \bar{\sigma}] \leftarrow \mathbf{x}$
  end while
  return $\boldsymbol{\sigma}, \bar{\sigma}$
end function

3.2. Inertial effects

3.2.1. Derivation

In the absence of an applied body force, the equation

$$\mathbf{f}_{inertia} + \mathbf{f}_{internal} = \mathbf{0} \tag{19}$$

summarizes the conservation of linear momentum. Here

$$\mathbf{f}_{internal} = \nabla \cdot \boldsymbol{\sigma}(\boldsymbol{\varepsilon}) \tag{20}$$

gives the internal body force, with $\boldsymbol{\sigma}(\boldsymbol{\varepsilon})$ the stress/strain relation derived above. The inertial force in the strut normal direction for a single strut is:

$$f_i = \int_0^{l_i} \rho_B A_i \ddot{u}_i(\xi_i) d\xi_i. \tag{21}$$

Assuming small deformations and a simple lattice, the Cauchy–Born assumption gives the joint accelerations as a function of the second time derivative of the applied strain

$$\ddot{\mathbf{u}} = \ddot{\boldsymbol{\varepsilon}} \cdot \mathbf{x}. \tag{22}$$

This assumption – that the nodal accelerations are affine with the second time derivative of strain – limits the model to the non-dispersive, long wavelength limit and to simple lattices. Using $\ddot{u}_i = \ddot{\mathbf{u}} \cdot \mathbf{n}_i$ and Eq. (21), the contribution of a single strut to the inertial force of the periodic structure is

$$\mathbf{f}_i = \left(\int_0^{l_i} \rho_B A_i \mathbf{n}_i \cdot \ddot{\boldsymbol{\varepsilon}} \cdot \mathbf{x} d\xi_i \right) \mathbf{n}_i \tag{23}$$

including direction.

The inertial body force of the homogenized truss is the volume-average of the contributions of each strut in the unit cell:

$$\mathbf{f}_{inertia} = \frac{\rho_B}{V} \int_V \left(\int_0^{l_i} A_i \mathbf{n}_i \cdot \ddot{\boldsymbol{\varepsilon}} \cdot \mathbf{x} d\xi_i \right) \mathbf{n}_i dV. \tag{24}$$

The field variables are constant in the line integral over the struts:

$$\mathbf{f}_{inertia} = \frac{\rho_B}{V} \int_V \ddot{\boldsymbol{\varepsilon}} \cdot \mathbf{x} \cdot \left\{ \int_0^{l_i} A_i (\mathbf{n}_i \otimes \mathbf{n}_i) d\xi_i \right\} dV \tag{25}$$

$$\mathbf{f}_{inertia} = \frac{\rho_B}{V} \int_V l_i A_i \ddot{\boldsymbol{\varepsilon}} \cdot \mathbf{x} \cdot (\mathbf{n}_i \otimes \mathbf{n}_i) dV \tag{26}$$

Then by Eq. (22)

$$\mathbf{f}_{inertia} = \frac{\rho_B}{V} \int_V l_i A_i \ddot{\mathbf{u}} \cdot (\mathbf{n}_i \otimes \mathbf{n}_i) dV \tag{27}$$

Expressing the volume integral as a sum over the finite struts:

$$\mathbf{f}_{inertia} = \left\{ \frac{\rho_B}{V} \sum_{i=1}^{n_{struts}} l_i A_i (\mathbf{n}_i \otimes \mathbf{n}_i) \right\} \cdot \ddot{\mathbf{u}}. \tag{28}$$

Rearranging Eq. (28) yields the equation

$$\mathbf{f}_{inertia} = \rho \ddot{\mathbf{u}} - \frac{\rho_B}{V} \sum_{i=1}^{n_{struts}} l_i A_i (\mathbf{I} - \mathbf{n}_i \otimes \mathbf{n}_i) \cdot \ddot{\mathbf{u}} \tag{29}$$

which expresses the inertial force as the macroinertia minus a microinertial correction term. Note Eq. (28) can also be expressed in terms of the relative density

$$\mathbf{f}_{inertia} = \left\{ \rho_B \bar{\rho} \frac{\sum_{i=1}^{n_{struts}} l_i A_i (\mathbf{n}_i \otimes \mathbf{n}_i)}{\sum_{i=1}^{n_{struts}} l_i A_i} \right\} \cdot \ddot{\mathbf{u}}. \tag{30}$$

Alternatively, the microinertial part of Eq. (29) can be expressed as a fictitious stress instead of a modification to the standard inertial force:

$$\rho \ddot{\mathbf{u}} = \nabla \cdot \left\{ \boldsymbol{\sigma}(\boldsymbol{\varepsilon}) - \boldsymbol{\sigma}_\mu(\ddot{\boldsymbol{\varepsilon}}) \right\}. \tag{31}$$

with

$$\boldsymbol{\sigma}_\mu = \frac{1}{k^2} \frac{\rho_B}{V} \sum_{i=1}^{n_{struts}} l_i A_i (\mathbf{I} - \mathbf{n}_i \otimes \mathbf{n}_i) \cdot \ddot{\boldsymbol{\varepsilon}}. \tag{32}$$

Here all terms are defined previously, expect for k, the wavenumber of the response. Again, this can be expressed in terms of the relative density

$$\boldsymbol{\sigma}_\mu = \frac{\rho_B \bar{\rho}}{k^2} \frac{\sum_{i=1}^{n_{struts}} l_i A_i (\mathbf{I} - \mathbf{n}_i \otimes \mathbf{n}_i)}{\sum_{i=1}^{n_{struts}} l_i A_i} \cdot \ddot{\boldsymbol{\varepsilon}}. \tag{33}$$

The microinertial term developed here specifically for a truss lattice material resembles the result of applying the general theory developed by Fish et al. (2002b,a) and Fish et al. (2012) to the periodic truss system.

3.2.2. Analytical description of wave propagation

Consider the balance of momentum expressed as

$$\mathbf{f}_{inertia} + \mathbf{f}_{internal} = 0. \tag{34}$$

Substituting Eqs. (4) and (28) yields

$$\rho_B \bar{\rho} \hat{M}_{ij} \ddot{u}_j - \left(E \bar{\rho} \hat{C}_{ijkl} \varepsilon_{kl} \right)_{,j} = 0 \tag{35}$$

with $\hat{\mathbf{M}} = \rho_B \bar{\rho} \sum_{i=1}^{n_{struts}} l_i A_i (\mathbf{n}_i \otimes \mathbf{n}_i) / \sum_{i=1}^{n_{struts}} l_i A_i$. Carrying through the divergence operator and expanding the small strain tensor transforms the equation to

$$\rho_B \bar{\rho} \hat{M}_{ij} \ddot{u}_j - E \bar{\rho} \hat{C}_{ijkl} u_{k,jl} = 0 \tag{36}$$

Consider a plane wave solution to this equation of the form

$$u_k = U_k e^{i(k_l x_l - \omega t)} \tag{37}$$

where U_k is the amplitude, k_l is the wavevector, and ω is the frequency of the wave. Substituting this expression into the balance of momentum yields

$$\left(E \hat{C}_{ijkl} k_j k_l - \rho_B \omega^2 \hat{M}_{ik} \right) u_k = 0. \tag{38}$$

This generalized eigenvalue problem is the equivalent of the Christoffel equation for traditional elastic media and describes long wavelength wave propagation in the equivalent continuum. Finally, define the wavevector in terms of its magnitude, the wavenumber, and a direction so that $k_j = k n_j$ with n_j a unit vector. Then

$$\left(\hat{C}_{ijkl} n_j n_l - \frac{\rho_B}{E} \frac{\omega^2}{k^2} \hat{M}_{ik} \right) u_k = 0. \tag{39}$$

Solving this eigenvalue problem for a particular direction n_j gives the response of the equivalent media for plane wave propagation. The form of this equation illustrates several features of the dynamic response of the equivalent medium theory. The relative density $\bar{\rho}$ cancels from the expression. Therefore, subject to the assumptions made in the derivation, trusses with the same lattice structure and bulk material but different relative densities will have the same elastic wavespeeds. Also, this equation shows that in the long wavelength limit the response of the media is non-dispersive. Solutions to the generalized eigenvalue problem will be eigenvalues λ^2 describing the quantity $\frac{\rho_B}{E} \frac{\omega^2}{k^2}$. Therefore

$$\frac{\omega}{k} = \pm \lambda_i \sqrt{\frac{E}{\rho_B}} \tag{40}$$

so frequency and wavenumber are linearly related and the medium is non-dispersive. We can then identify the quantity ω/k as c, the velocity of wave propagation, without needing to distinguish between the phase and group velocities. The propagation speed of an elastic wave in the equivalent medium is then some factor times the bar wavespeed of the bulk material

$$c = \lambda_i c_{bar} \tag{41}$$

with $c_{bar} = \sqrt{E/\rho_B}$. Eq. (39) has dimension three, and so the medium can have up to three propagation modes – one quasi-longitudinal and two quasi-transverse.

The alternative statement of the microinertial correction as a fictitious stress produces the same dynamic response. Again start with the balance of linear momentum, but now substitute Eq. (33) instead of Eq. (28):

$$\rho_B \bar{\rho} \ddot{u}_i - \left(E\bar{\rho}\hat{C}_{ijkl}\varepsilon_{kl} - \frac{\rho_B \bar{\rho}}{k^2}\left(\delta_{ik} - \hat{M}_{ik}\right)\ddot{\varepsilon}_{kj}\right)_{,j} = 0 \tag{42}$$

with $\hat{\mathbf{M}} = \rho_B \bar{\rho} \sum_{i=1}^{n_{struts}} l_i A_i (\mathbf{n}_i \otimes \mathbf{n}_i) / \sum_{i=1}^{n_{struts}} l_i A_i$ as previously. Expanding the equation in terms of the plane wave solution yields

$$(E\bar{\rho}\hat{C}_{ijkl}k_j k_l - \omega^2 \frac{\rho_B \bar{\rho}}{k^2}\left(\delta_{ik} - \hat{M}_{ik}\right)k_j k_j - \rho_B \bar{\rho}\omega^2)u_k = 0 \tag{43}$$

Again substituting $k_j = k n_j$ and simplifying:

$$\left(\hat{C}_{ijkl}n_j n_l - \frac{\rho_B}{E}\frac{\omega^2}{k^2}\hat{M}_{ik}\right)u_k = 0. \tag{44}$$

This is identical to Eq. (39), showing the stress correction is consistent with the direct correction to the inertial force.

3.2.3. Implementation of the microinertial correction

Depending on the application, there may be advantages to implementing either Eq. (29) or Eq. (31).

As described in the previous section, Eq. (29) is preferable when calculating the elastic wavespeeds in the homogenized system via the Christoffel equation. The standard eigenvalue problem

$$(C_{ijkl}n_j n_l - \omega^2 \rho \delta_{ik})p_k = 0 \tag{45}$$

with C_{ijkl} the (effective) elastic stiffness, n_j the direction, ω the frequency, and p_k the polarization vector becomes the generalized eigenvalue problem

$$(C_{ijkl}n_j n_l - \omega^2 G_{ik})p_k = 0 \tag{46}$$

with $G_{ik} = \frac{\rho_B}{V}\sum_{s=1}^{n_{bars}} l^{(s)} A^{(s)} n_i^{(s)} n_j^{(s)}$.

For implicit finite elements Eq. (28) may also be preferable. The inertial term (mass matrix) of the standard, implicit Galerkin discretization for the unknown accelerations $\ddot{d}_j$ with shape functions N_{ij}

$$\mathbf{f}_{inertia} = \int_\Omega \rho N_{ik} N_{kj} d\Omega \ddot{d}_j \tag{47}$$

becomes

$$\mathbf{f}_{inertia} = \int_\Omega \rho N_{ik} G_{kl} N_{lj} d\Omega \ddot{d}_j \tag{48}$$

with

$$\mathbf{G} = \frac{\rho_B}{V}\sum_{i=1}^{n_{struts}} l_i A_i (\mathbf{n}_i \otimes \mathbf{n}_i). \tag{49}$$

Therefore, implementing the microinertial correction requires only changing the definition of the mass matrix.

In explicit finite element formulations or in implicit finite element implementations where altering the mass matrix is difficult Eq. (31) becomes preferable. In these situations the microinertial correction can be implemented as a fictitious stress calculated during the material stress update. At a minimum, a finite element framework will provide a material model with the strain at the new and previous time steps and the set of history variables at the previous time step. The model must return the updated stress:

$$\boldsymbol{\sigma}_{n+1} = \boldsymbol{\sigma}(\boldsymbol{\varepsilon}_{n+1}, \boldsymbol{\varepsilon}_n, \mathbf{s}_n). \tag{50}$$

To implement the microinertial correction the material model instead returns

$$\boldsymbol{\sigma}_{n+1} = \boldsymbol{\sigma}(\boldsymbol{\varepsilon}_{n+1}, \boldsymbol{\varepsilon}_n, \mathbf{s}_n) + \frac{1}{k^2}\frac{\rho_B}{V}\sum_{i=1}^{n_{struts}} l_i A_i (\mathbf{I} - \mathbf{n}_i \otimes \mathbf{n}_i)\cdot \ddot{\boldsymbol{\varepsilon}}_{n+1}. \tag{51}$$

The finite element framework typically will not know *a priori* the wavenumber k of the response. Instead, the implementation might focus on certain critical wave numbers that give a good representation of the dispersion relation of the effective medium. For lattice materials a good heuristic for choosing critical values of the wavenumber might be to select waves with wave vectors aligned with the reciprocal lattice. For a cubic lattice this choice yields $1/k^2 = a^2$, with a the lattice parameter.

The update further requires the second time derivative of the strain $\ddot{\boldsymbol{\varepsilon}}_{n+1}$, typically not available to a finite element (FE) material model. The material model could construct the time derivative via the differencing scheme

$$\ddot{\boldsymbol{\varepsilon}}_{n+1} = \frac{\dot{\boldsymbol{\varepsilon}}_{n+1} - \dot{\boldsymbol{\varepsilon}}_n}{\Delta t_{n+1}}. \tag{52}$$

This scheme requires the rate of strain at the previous time step as an additional history variable. If the finite element formulation does not provide the strain rate, it can be calculated again by differencing as

$$\dot{\boldsymbol{\varepsilon}}_{n+1} = \frac{\boldsymbol{\varepsilon}_{n+1} - \boldsymbol{\varepsilon}_n}{\Delta t_{n+1}}. \tag{53}$$

4. Example analyses: the octet truss

In this work the octet truss (Fuller, 1961) serves as an exemplar for stretch-dominated lattice materials. Previous research describes the elastic and plastic properties of periodic octet truss structures (Deshpande et al., 2001; Elsayed and Pasini, 2010). Fig. 1 shows the unit cell of the octet truss geometry. The direct lattice vectors correspond to the cartesian coordinate system shown on the figure. Consider an infinite, periodic octet truss comprised of struts of equal cross-sectional area A and Young's modulus E. The approximate relative density of this truss is:

$$\bar{\rho} = \frac{6\sqrt{2}A}{l^2}. \tag{54}$$

Following the procedure summarized in Section 2 leads to the effective elastic stiffness (in Voigt notation):

$$\boldsymbol{\sigma} = \mathbf{C}\cdot\boldsymbol{\varepsilon} \tag{55}$$

$$\begin{bmatrix}\sigma_{11}\\ \sigma_{22}\\ \sigma_{33}\\ \sigma_{23}\\ \sigma_{13}\\ \sigma_{12}\end{bmatrix} = E\bar{\rho}\begin{bmatrix}\frac{1}{6} & \frac{1}{12} & \frac{1}{12} & 0 & 0 & 0\\ \frac{1}{12} & \frac{1}{6} & \frac{1}{12} & 0 & 0 & 0\\ \frac{1}{12} & \frac{1}{12} & \frac{1}{6} & 0 & 0 & 0\\ 0 & 0 & 0 & \frac{1}{12} & 0 & 0\\ 0 & 0 & 0 & 0 & \frac{1}{12} & 0\\ 0 & 0 & 0 & 0 & 0 & \frac{1}{12}\end{bmatrix}\begin{bmatrix}\varepsilon_{11}\\ \varepsilon_{22}\\ \varepsilon_{33}\\ 2\varepsilon_{23}\\ 2\varepsilon_{13}\\ 2\varepsilon_{12}\end{bmatrix} \tag{56}$$

and the procedure described in Section 3.2 produces the inertial body force, including microinertial terms:

$$\mathbf{f}_{inertia} = \rho_B \bar{\rho} \begin{bmatrix} \frac{1}{3} & 0 & 0 \\ 0 & \frac{1}{3} & 0 \\ 0 & 0 & \frac{1}{3} \end{bmatrix} \cdot \ddot{\mathbf{u}} \tag{57}$$

where ρ_B is the bulk density of the strut material. Note for this particular periodic truss the inertial force can be expressed as

$$\mathbf{f}_{inertia} = \frac{1}{3} \rho_B \bar{\rho} \ddot{\mathbf{u}}. \tag{58}$$

The physical mass density of the infinite truss is $\rho = \rho_B \bar{\rho}$. Therefore, the effective inertial density of the truss is one-third of its physical mass density – with microinertial effects generating the difference between the physical and effective inertial density. Implementing the microinertial correction to the octet truss requires only reducing the inertial density of the equivalent continuum by two-thirds.

The stiffness matrix (Eq. (56)) of the octet truss has cubic symmetry. This implies the elastic properties of the octet truss are anisotropic. The plastic response of the octet is similarly anisotropic. Therefore, the results presented below depend on the orientation of the octet relative to the applied loading. All the load cases described below are uniaxial deformations after rotation of the truss. A crystallographic-type system describes the orientation of the octet after rotation. Fig. 1 shows a 1 0 0 orientation. A 1 1 0 orientation rotates the octet so that the image of the x-axis lies along the line described by the vector $[1 \quad 1 \quad 0]$ in the original coordinates. Similarly, a 1 1 1 orientation rotates the octet so that the image of the x-axis lies along the line described by the vector $[1 \quad 1 \quad 1]$ in the original coordinates.

4.1. Static analysis

Fig. 4 shows one of three meshes used to verify the equivalent continuum model described in this work against detailed finite element models in quasi-static conditions. The three meshes have the same basic structure but vary the radius of the struts to change the overall relative density of the unit cell ($\bar{\rho} = 0.1, 0.3, 0.5$). The FE models are loaded with applied displacements in the x-direction and are under symmetry boundary conditions in the y- and z-directions. The FE analyses are run with WARP3D, an open-source, implicit Lagrangian, nonlinear finite element program (http://www.warp3d.net/). The equivalent applied strain is

$$\varepsilon = \frac{\Delta d_{applied}}{s} \tag{59}$$

with $d_{applied}$ the applied displacement and s the length of the unit cell, here $s = \sqrt{2}l = 0.294$ mm. Define the equivalent stress as the volume average of the stress in each element over the total unit cell

$$\boldsymbol{\sigma} = \frac{1}{V} \int_{\Omega} \boldsymbol{\sigma}_e dV. \tag{60}$$

The material model used in the FE simulation is bilinear plasticity, with Young's modulus E, Poisson's ratio v, yield stress σ_0, and plastic hardening modulus H. Table 1 summarizes the material properties.

For direct comparison to the FE models, the material model described in this work is driven with the (Voigt notation) strain vector

$$\boldsymbol{\varepsilon} = [\varepsilon \quad 0 \quad 0 \quad 0 \quad 0 \quad 0]. \tag{61}$$

The material properties are the same as for the FE simulations, listed in Table 1, except the Poisson's ratio v is not a parameter of the equivalent truss model.

Fig. 5 shows a series of stress–strain curves comparing the equivalent continuum model to the finite element simulations. At low values of relative density the equivalent continuum model agrees with the FE results. As the relative density of the truss increases the equivalent continuum model becomes less and less accurate. Fig. 6 explains this trend. The figure shows the axial stress in a strut of the finite element model for the three different values of relative density all at the same strain. The equivalent model assumes the structure behaves as an ideal truss – that bending deformation does not occur in the struts. As Fig. 6 shows, this assumption holds at lower values of relative density. The normal stress profile for $\bar{\rho} = 0.1$ is nearly a horizontal line – implying zero bending moment and zero corresponding bending deformation. As the relative density of the lattice increases the amount of bending moment in the strut increases – that is, the struts transmits load through a combination of axial force and bending shear and moment. This invalidates the assumption of the equivalent continuum truss model and produces the reduction in accuracy shown in Fig. 5.

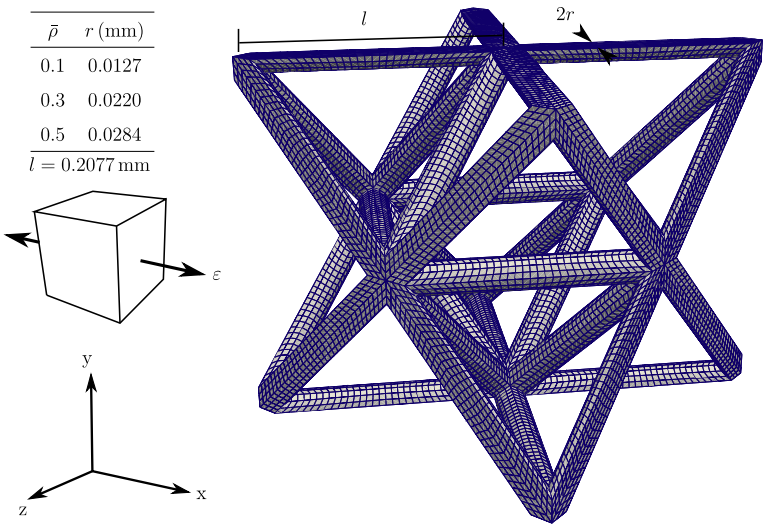

Fig. 4. One of three meshes used for verifying the quasi-static properties of the reduced model against full finite element simulations. For all simulations $l = 0.2077$ mm, which also fixes the size of the unit cell. Each simulation has a different strut radius r to target a particular value of relative density ($\bar{\rho}$). Changing the strut radius affects the discretization, but all meshes have approximately 30,000 elements and 40,000 nodes.

Table 1
Material properties for the finite element simulations and (excepting Poisson's ratio ν) the equivalent continuum truss model.

Property	Description	Value
E	Young's modulus	1780 MPa
ν	Poisson's ratio	0.35
σ_0	Yield stress	40 MPa
H	Hardening modulus	100 MPa
ρ_B	Strut density	1.18 g/cm^3

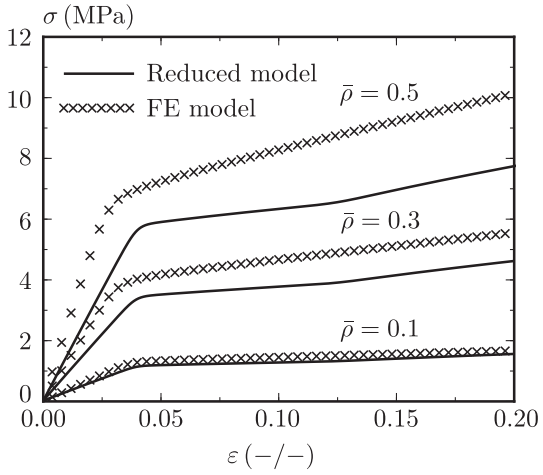

Fig. 5. Uniaxial deformation, 100-direction tension stress/strain curves for the octet truss at different relative densities. The plot compares the reduced model developed here to full finite element simulations of an octet truss unit cell.

Two factors determine the amount of bending deformation relative to axial deformation for a strut and joint structure. The first factor is whether or not the structure is stable when analyzed as a pin-jointed truss. This depends on the connectivity of the joints, essentially an extension of Maxwell's rule to periodic trusses (Hutchinson and Fleck, 2006). If the structure is not stable as a truss then bending in the struts is required for structural stability – these are the classical bend-dominated lattices. Lattices that are stable analyzed as trusses are the classical stretch-dominated lattices, like the octet truss. However, even in stretch dominated lattices, the amount of axial deformation relative to bending deformation in the lattice is controlled by the joint stiffness. If the joints are flexible then the lattice will tend to deform as if the struts were joined by hinges. A hinged structure will deform as a truss, with the struts in axial tension or compression. If the joints are stiff then the structure will tend to deform as a frame with combined flexural and axial deformation.

Approximating the joints as small flexural members, the joint stiffness scales as $k_j \sim Ed^3$ with E the Young's modulus and d the section height. The relative density scales as $\bar{\rho} \sim d^2/l$ with l the strut length. For a fixed unit cell size increasing the relative density requires increasing the section height d. Since the relative density scales as d^2 and the joint stiffness scale as d^3, trusses with higher relative densities will have much higher joint stiffnesses, leading to non-axial deformation, invalidating the assumptions of truss theory. The finite element simulations demonstrate this trend. The relative density can also be increased by making the strut length l smaller. Then the joint stiffness remains constant and the lattice can continue to deform as a stretch dominated truss, even at high relative density. However, the manufacturing process typically imposes some lower bound to the unit cell size. For structures with unit cells at this lower bound, the only option is to increase the strut height (Meza et al., 2014; Schaedler et al., 2011).

Fig. 7 shows the effect of truss orientation on the quasi-static stress–strain curves generated by the equivalent continuum model. These curves are for octet lattices at 10% relative density. Both the elastic and plastic properties are anisotropic. In the elastic regime, the 111 orientation has the highest stiffness, followed by the 110, and 100 orientations. This follows from the structure of the cubic equivalent elasticity tensor and the general tend has been observed by other researchers (Deshpande et al., 2001; Johnston et al., 2006). For plasticity the directional effects are more complicated. The 100 orientation has the highest yield stress followed by the 111 and 110 orientations. Examining the rotation of the struts relative to the applied loading for each different truss orientation reveals the cause of this trend in the yield stress. In the 110 orientation a family of struts aligns directly with the loading axis, resolving a large amount of strut tension. This causes those struts to yield under comparatively little applied load, decreasing the macroscale, equivalent yield stress. In the 100 orientation all struts are substantially misaligned with the applied loading, resolving relatively little tension and requiring more applied load to yield. The orientation of the truss also effects the slope of the macroscale hardening curve. Load redistribution in the struts can cause a kink in the hardening curve. For the 111 orientation load redistribution actually causes macroscale softening, before additional redistribution returns the curve to hardening.

4.2. Wave propagation

4.2.1. Bloch wave theory

The Bloch wave theory describes the propagation of plane waves in a periodic medium, including dispersion and attenuation (Bloch, 1928). The model developed here provides the response of a periodic, stretch lattice material as an equivalent continuum in the long wavelength limit. As such, it is a special case of the Bloch theory and both methods should agree for long wavelengths.

Srikantha Phani et al. (2006) previously described the dynamics of wave propagation of 2D lattice materials using the Bloch wave theory. The extension to 3D lattices is straightforward and briefly summarized here. Consider a unit cell of a periodic lattice material, as described above. Applying the theory of structural trusses to the unit cell results in a discrete system of equations representing conservation of momentum for unforced, undamped motion

$$\mathbf{M} \cdot \ddot{\mathbf{u}} + \mathbf{K} \cdot \mathbf{u} = \mathbf{0} \tag{62}$$

where $\mathbf{M}$ is a discrete mass matrix, $\mathbf{K}$ a discrete stiffness matrix, and $\mathbf{u}$ the discrete displacement vector concatenating the displacements of each joint in the unit cell.

Bloch's theorem gives the solution for a plane wave propagating across the infinite, periodic medium in terms of the unit cell. For simple lattices, where all joint positions are lattice points, the Bloch theorem ties the displacements of the joints together by a spatial phase shift. The procedure is to choose a single, arbitrary joint in the unit cell $\mathbf{u}_i$ to be a free displacement and tie the remaining joint displacements to it by the phase shift

$$\mathbf{u}_j = \mathbf{u}_i e^{i\mathbf{k}\cdot(\mathbf{x}_j - \mathbf{x}_i)}. \tag{63}$$

In this expression $\mathbf{k}$ is the wave vector of the plane wave propagating through the periodic medium and $\mathbf{x}_j$ and $\mathbf{x}_i$ are the joint positions. This transformation reduces the full unit cell displacement vector down to a constrained set of joint displacements

$$\hat{\mathbf{u}} = \mathbf{T}^H(\mathbf{k}) \cdot \mathbf{u} \tag{64}$$

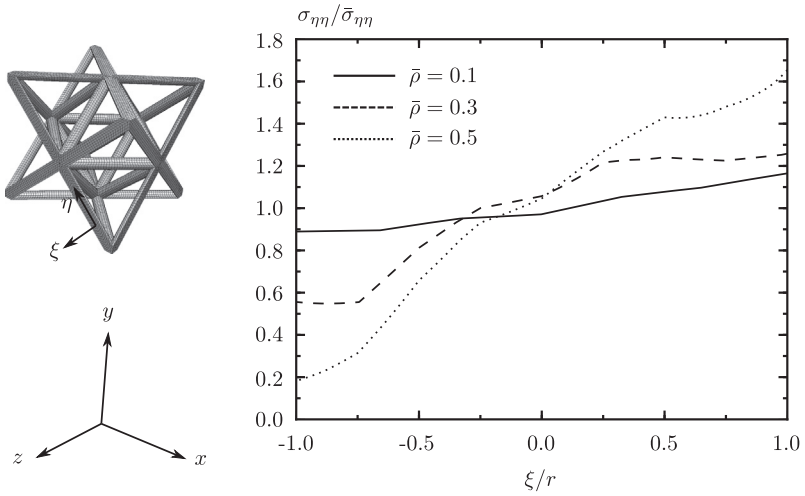

Fig. 6. Axial stress ($\sigma_{\eta\eta}$) in the finite element models, normalized by the average axial stress across the strut ($\bar{\sigma}_{\eta\eta}$), versus position across the strut, normalized by the strut radius, for three different values of relative density. The center of the strut is at $\xi = 0$. The coordinate system is positioned at the quarter point of the indicated strut. With this normalization pure axial deformation is a straight line at $\sigma_{\eta\eta}/\bar{\sigma}_{\eta\eta} = 1.0$. The plot shows that the amount of bending moment in the strut increases as the relative density of the truss increases.

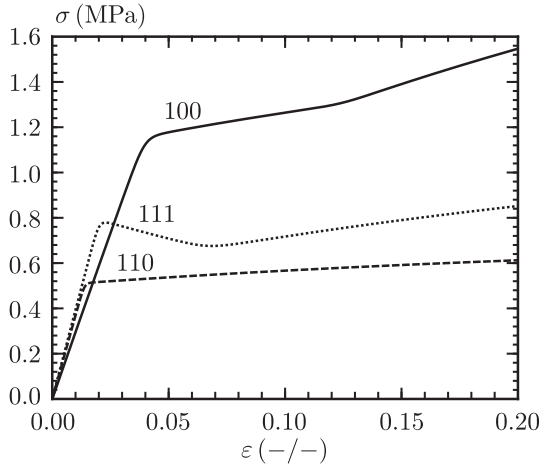

Fig. 7. Uniaxial deformation stress/strain curves for the octet truss at 10% relative density in three different directions: 100, 110, and 111.

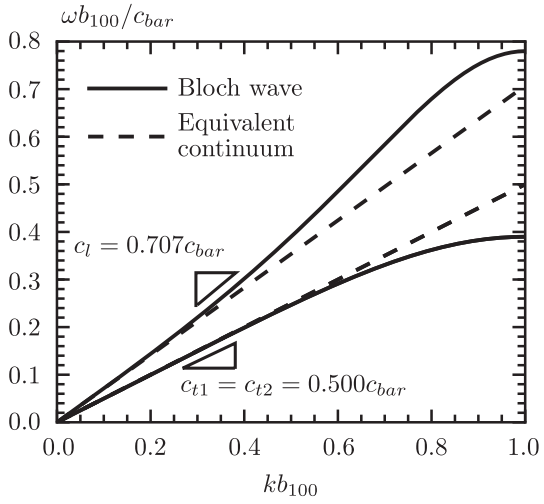

Fig. 8. Plot comparing the dispersion relation predicted by the Bloch wave theory to the dispersion relation predicted by the equivalent continuum model developed in this work for plane waves propagating in the 100 direction. b_{100} is the length of the first Brillouin zone in the 100 direction, $b_{100} = \left(\pi\sqrt{2}l\right)^{-1}$. The plot is normalized so that the slope of a line gives the group velocity in terms of the bulk bar wave speed $c_{bar} = \sqrt{E/\rho_B}$.

where $\mathbf{T}(\mathbf{k})$ is a transformation matrix which varies with the wave vector $\mathbf{k}$ and H denotes the conjugate transpose operator. A similar transformation applies to the strut forces. Applying these transformations to Eq. (62) yields

$$\hat{\mathbf{M}}(\mathbf{k}) \cdot \ddot{\hat{\mathbf{u}}} + \hat{\mathbf{K}}(\mathbf{k}) \cdot \hat{\mathbf{u}} = \mathbf{0} \tag{65}$$

with $\hat{\mathbf{M}}(\mathbf{k}) = \mathbf{T}^H(\mathbf{k}) \cdot \mathbf{M} \cdot \mathbf{T}(\mathbf{k})$ and $\hat{\mathbf{K}}(\mathbf{k}) = \mathbf{T}^H(\mathbf{k}) \cdot \mathbf{K} \cdot \mathbf{T}(\mathbf{k})$. The plane wave solution to this equation describes the propagation of a phase-shifted wave with wave vector $\mathbf{k}$ and frequency ω propagating across the infinite, periodic medium. This solution takes the form of the generalized eigenvalue problem

$$\left(\hat{\mathbf{K}}(\mathbf{k}) - \omega^2 \hat{\mathbf{M}}(\mathbf{k})\right) \cdot \hat{\mathbf{u}} = \mathbf{0}. \tag{66}$$

Given a wave vector $\mathbf{k}$, the eigenvalues of this equation ω^2 give the frequencies at which that wave can propagate.

Fig. 8 shows the full response spectrum – the dispersion relation for all modes – for plane waves propagating through the infinite, periodic octet truss with wavevectors in the 100 direction. That is, $\mathbf{k} = k\mathbf{n}$ with k the wavenumber and $\mathbf{n}$ the unit vector in the direction of 100. The abscissa of the plot contains the first Brillouin zone in the 100 direction – sufficient to fully capture the response. Figs. 9 and 10 show similar plots for the 110 and 111 directions.

The Bloch wave response of the periodic octet is dispersive. Therefore, equivalently:

1. The relation between wave number k and frequency ω is nonlinear.
2. Unlike the long wavelength limit discussed in Section 3.2.2, a single velocity no longer describes the propagation of a wave. A given point on the waveform propagates at the phase velocity $v_p = \omega/k$ while the modulation – the energy contained in the waveform – propagates at the group velocity $v_g = \partial\omega/\partial k$.
3. The velocity of a wave varies with its frequency. Or, equivalently, the velocity of a wave varies with its wave number.

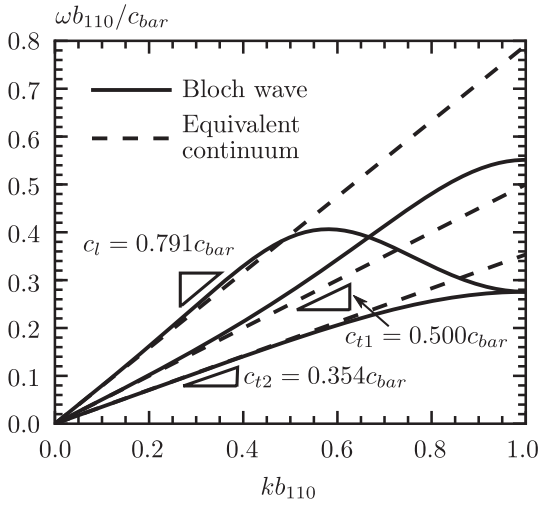

Fig. 9. Plot similar to Fig. 8 but for the 1 1 0 direction. b_{110} is the length of the first Brillouin zone in the 1 1 0 direction, $b_{110} = (2\pi l)^{-1}$.

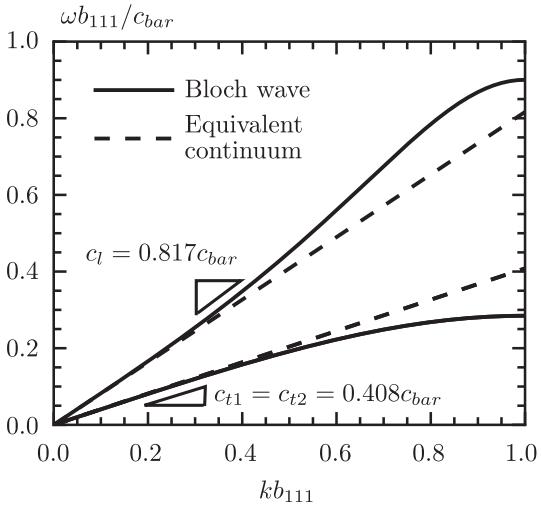

Fig. 10. Plot similar to Fig. 8 but for the 1 1 1 direction. b_{111} is the length of the first Brillouin zone in the 1 1 1 direction, $b_{111} = \left(\sqrt{6}\pi l/2\right)^{-1}$.

The figures also plot the dispersion relation predicted by the equivalent continuum theory, as summarized by Eq. (39). Both theories predict three modes of propagation – one longitudinal (speed c_l) and two transverse (speeds c_{t1} and c_{t2}). The continuum theory exactly matches the wave speeds predicted by the full Bloch wave analysis at small values of the wavenumber k – that is, long wavelengths. Furthermore, for the octet, the predicted dispersion is minimal for waves with wavelengths greater than about half the lattice spacing. In this range of wavelengths the non-dispersive equivalent continuum theory provides a good estimate for the response of the periodic structure.

4.2.2. Finite element simulations of wave propagation

Comparison to the Bloch wave analysis shows that the equivalent continuum model is accurate for harmonic motion with long wavelengths. The continuum model also accurately represents the propagation of other waveforms that are well represented by a plane wave expansion concentrated around low wave numbers. One waveform with such properties is the step function. The Fourier transform of a propagating step into wave number space is proportional to $1/k$, suggesting long wavelength modes will govern the propagation of the wave.

The propagation of a step wave is significant because impact loading can be idealized as a step function in the velocity applied to a structure. Fig. 11 shows a 3D finite element simulation designed to verify the equivalent continuum model against the response of a 1 0 0-direction step wave propagating in a periodic octet lattice. The model consists of 16 octet unit cells stacked in the x-direction. The material model is bilinear plasticity with the same properties listed in Table 1. At $t = 0$ the nodes on the left of the lattice are set to move to the right at an initial velocity v_0. The simulation has boundary conditions enforcing periodicity in the y- and z-directions and the simulation halts before a wave reaches the far boundary along the x-axis. The FE simulations were run with ALE3D, an arbitrary Lagrangian–Eulerian finite element code developed at Lawrence Livermore National Laboratory (Nichols, 2014).

The initial velocity v_0 is calibrated to result in moderate plastic deformation in the lattice and to avoid localization and collapse of the lattice structure. Fig. 11 shows the deformed configuration of the mesh at $t = 12.8$ μs after the application of a step with amplitude $v_0 = 20$ m/s. While the lattice does deform plasticity it does not collapse. In its final configuration it still has the structure of a periodic lattice, so the assumptions of the equivalent continuum theory remain valid.

The lattice responds to the step loading by propagating a wave. The fringe in Fig. 11 shows the material velocity in the impact direction ($\dot{x}$) and indicates the position of the wave front. As the wave propagates it does not remain an ideal step, jumping from $\dot{x} = 0$ to $\dot{x} = v_0$ in zero time and distance, but instead spreads out in time and space and decreases in amplitude, as indicated on the figure. This represents attenuation and dispersion of the wave caused by both the lattice structure and the artificial viscosity necessary for a stable numerical simulation. However, because the plane wave expansion of a step wave concentrates in the low wave number, non-dispersive region the waveform remains relatively compact as it travels.

Fig. 12 plots the position of the wave in time as it travels across the lattice. This plot refers to a series of tracer particles embedded in the model, spread out in the x-direction and located at lattice points. Fig. 11 shows the location of these tracers. The x-coordinate of the tracers defines the ordinate of the points show in the plot. The abscissa of the points is the time at which the wavefront reaches a given tracer particle, as defined by the particle beginning to move – developing some non-zero $\dot{x}$. As the plot shows, the wave slows as it travels, representing some dispersion in the simulation. However, over the first seven unit cells, which is approximately the position of the wave indicated in Fig. 11, dispersion has not significantly slowed the wave front. This is indicated by the linear fit to the data shown in Fig. 12 – a linear fit on this plot represents steady wave propagation. The slope of the line gives the velocity of the wave front, $c_{FEM} = 0.72 c_{bar}$. This speed matches the speed predicted by the equivalent continuum model via Eq. (39) and shown in Fig. 8 – $c_{model} = 0.71 c_{bar}$.

If the amplitude of the initial step v_0 increases the lattice responds differently. Instead of propagating a step wave the lattice structure collapses and a shock develops. Previous experiments on similar materials show that the propagation of the shock is governed by the localization and compaction of the material structure (Barnes et al., 2014; Gaitanaros and Kyriakides, 2014). In the simulations the onset of this localization is plastic buckling of the struts. Localization in the material breaks the assumptions of classic periodic homogenizations like the one used here to generate the equivalent continuum theory. Therefore, the equivalent continuum approach will not accurately describe the development and propagation of the shock.

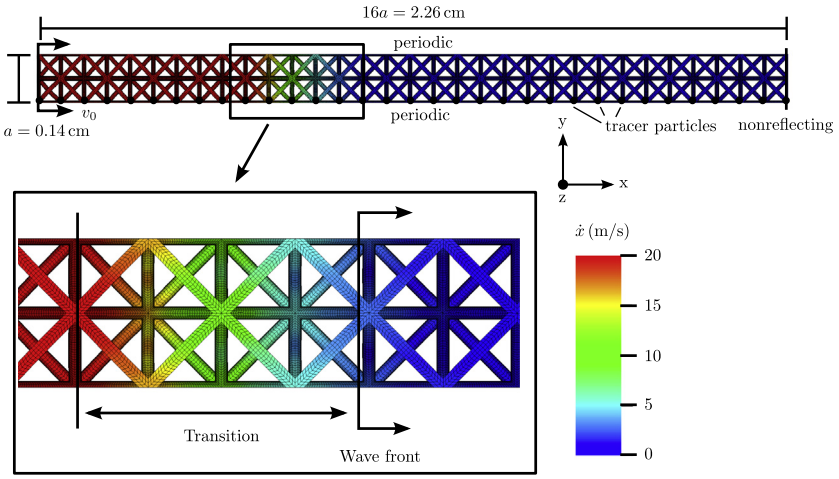

Fig. 11. Finite element simulation designed to verify the continuum model against the propagation of a step wave through an octet lattice in the 100 direction. The figure shows the deformed mesh at $t = 12.8$ μs after the application of $v_0 = 20$ m/s to the nodes on the left of the model. The fringe colors show the material velocity in the x-direction, indicating the position of the propagating wave front.

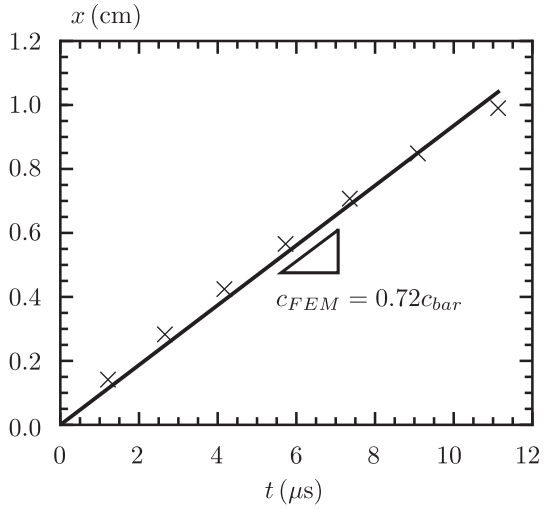

Fig. 12. Plot calculating the speed of the step wave propagating across the simulation in the 100 direction. Data points give the position of the wave front versus time, the slope of the linear fit gives the speed.

5. Conclusions

The key contributions of this work are:

- An equivalent continuum model for periodic truss structures that captures the response of the material for wave propagation at long wavelengths.
- Verification of the model against the dynamic response predicted by the Bloch wave theorem and against detailed finite element calculations.
- For simple lattices, an expression for the axial stress resolved in each strut that preserves joint equilibrium under arbitrary loadings.
- Overcoming the problem of vertices on the equivalent yield surface by incorporating moderate rate sensitivity. Crystal plasticity models inspire this solution. The work draws other connections between crystal plasticity and equivalent truss models.
- A novel expression for the inertial body force of a periodic truss that correctly accounts for microinertial effects. Accurate calculation of long wavelength characteristics, such as the elastic sound speed, requires these microinertial corrections in addition to the correct effective elastic stiffness tensor.

The equivalent continuum model developed here is suitable for implementation as a standard material model in a finite element code for low density lattices at moderate strains. The model will capture the long wavelength response of the periodic structure, neglecting dispersion and attenuation. Such an implementation can correctly handle boundary effects and more general loadings than the verification examples presented here. For simple lattices, the small deformation model described in this work also easily extends to large deformations via a process analogous to how crystal plasticity models extend to large lattice deformations.

Acknowledgments

This work was performed under the auspices of the U.S. Department of Energy by Lawrence Livermore National Laboratory under Contract DE-AC52-07NA27344 (LLNL-JRNL-667808). The authors thank Greg Schebler for creating the meshes used for the finite element calculations.

Appendix A. Material Jacobian

Algorithm 1 poses the material model developed in this work as the solution to a set of nonlinear residual equations $\mathbf{R}_{n+1} = \mathbf{0}$. Solving these equations via the Newton–Raphson method requires the Jacobian matrix $\partial \mathbf{R}_{n+1}/\partial \mathbf{x}_{n+1}$, where $\mathbf{x}_{n+1}$ is the vector of unknown variables, here $[\boldsymbol{\sigma}_{n+1} \quad \bar{\sigma}_{n+1}]^T$, with $\boldsymbol{\sigma} = [\sigma_{xx} \quad \sigma_{yy} \quad \sigma_{zz} \sigma_{yz} \sigma_{xz} \sigma_{xy}]^T$. Based on the structure of the residual equations the Jacobian matrix divides into blocks of the form

$$\mathbf{J} = \begin{bmatrix} \mathbf{J}_{11} & \mathbf{J}_{12} \\ \mathbf{J}_{21} & J_{22} \end{bmatrix}.$$

The following equations give each block:

$$\mathbf{J}_{11} = (1 + \mathrm{tr}\Delta\boldsymbol{\varepsilon}^p)\mathbf{I} + \frac{n\Delta\varepsilon_0}{\bar{\sigma}^n \bar{\rho}} \boldsymbol{\sigma} \otimes \left\{ \sum_{i=1}^{n_{struts}} |\sigma_i|^{n-1} \hat{\mathbf{C}}^{-1} \cdot (\mathbf{n}_i \otimes \mathbf{n}_i) \right\} + \frac{En\Delta\varepsilon_0}{\bar{\sigma}^n} \hat{\mathbf{C}} \cdot \left[\sum_{i=1}^{n_{struts}} |\sigma_i|^{n-1} (\mathbf{n}_i \otimes \mathbf{n}_i) \otimes \left\{ \hat{\mathbf{C}}^{-1} \cdot (\mathbf{n}_i \otimes \mathbf{n}_i) \right\} \right]$$

$$\mathbf{J}_{12} = -\frac{n}{\bar{\sigma}} \left(\boldsymbol{\sigma} \sum_{i=1}^{n_{bars}} \Delta\varepsilon_i + \bar{\rho} E \hat{\mathbf{C}} \cdot \Delta\boldsymbol{\varepsilon}^p \right)$$

$$\mathbf{J}_{21} = -\frac{Hn\Delta\varepsilon_0}{\bar{\sigma}^n \bar{\rho}} \sum_{i=1}^{n_{struts}} |\sigma_i|^{n-2} \sigma_i \hat{\mathbf{C}}^{-1} \cdot (\mathbf{n}_i \otimes \mathbf{n}_i)$$

$$J_{22} = 1 + \frac{Hn}{\bar{\sigma}} \sum_{i=1}^{n_{struts}} |\Delta\varepsilon_i|$$

In these expressions $\Delta\varepsilon_i = \dot{\varepsilon}_i \Delta t = \Delta\varepsilon_0 \left|\frac{\sigma_i}{\bar{\sigma}_i}\right|^{n-1} \frac{\sigma_i}{\bar{\sigma}_i}$.

References

Asaro, R.J., 1983. Micromechanics of crystals and polycrystals. Adv. Appl. Mech. 23, 1–115.

Barnes, A.T., Ravi-Chandar, K., Kyriakides, S., Gaitanaros, S., 2014. Dynamic crushing of aluminum foams: part I – experiments. Int. J. Solids Struct. 51 (9), 1631–1645.

Bishop, J., Hill, R., 1951a. A theoretical derivation of the plastic properties of a polycrystalline face-centred metal. Philos. Mag. 42 (334), 1298–1307.

Bishop, J., Hill, R., 1951b. A theory of the plastic distortion of a polycrystalline aggregate under combined stresses. Philos. Mag. 42 (327), 414–427.

Bloch, F., 1928. Über die Quantenmechanik der Elektronen in Kristallgittern. Z. Phys. 52, 555–599.

Deshpande, V., Fleck, N., Ashby, M., 2001. Effective properties of the octet-truss lattice material. J. Mech. Phys. Solids 49 (8), 1747–1769.

Elsayed, M.S., Pasini, D., 2010. Multiscale structural design of columns made of regular octet-truss lattice material. Int. J. Solids Struct. 47 (14–15), 1764–1774.

Evans, A., Hutchinson, J., Fleck, N., Ashby, M., Wadley, H., 2001. The topological design of multifunctional cellular metals. Prog. Mater. Sci. 46 (3–4), 309–327.

Fish, J., Chen, W., Nagai, G., 2002a. Non-local dispersive model for wave propagation in heterogeneous media: multi-dimensional case. Int. J. Numer. Methods Eng. 54 (3), 347–363.

Fish, J., Chen, W., Nagai, G., 2002b. Non-local dispersive model for wave propagation in heterogeneous media: one-dimensional case. Int. J. Numer. Methods Eng. 54 (3), 331–346.

Fish, J., Filonova, V., Kuznetsov, S., 2012. Micro-inertia effects in nonlinear heterogeneous media. Int. J. Numer. Methods Eng. 91 (13), 1406–1426.

Forest, S., Pilvin, P., 1999. Modelling finite deformation of polycrystals using local objective frames. Z. Angew. Math. Mech. 79, 199–202.

Fuller, R.B., 1961. Octet truss.

Gaitanaros, S., Kyriakides, S., 2014. Dynamic crushing of aluminum foams: part II – analysis. Int. J. Solids Struct. 51 (9), 1646–1661.

Hill, R., Rice, J., 1972. Constitutive analysis of elastic-plastic crystals at arbitrary strain. J. Mech. Phys. Solids 20 (6), 401–413.

Howard, S.M., Pao, Y.-H., 1998. Analysis and experiments on stress waves in planar trusses. J. Eng. Mech. 124 (8), 884–891.

Hutchinson, R., Fleck, N., 2006. The structural performance of the periodic truss. J. Mech. Phys. Solids 54 (4), 756–782.

Johnston, S.R., Rosen, D.W., Reed, M., Wang, H.V., 2006. Analysis of mesostructure unit cells comprised of octet-truss structures. In: Proc. Seventeenth Solid Free. Fabr. Symp. Austin, TX.

Kocks, U.F., 1998. Kinematics and kinetics of plasticity. In: Kocks, U.F., Tome, C.N., Wenk, H.-R. (Eds.), Texture and Anisotropy. Ch. 8, pp. 327–389.

Kruth, J.-P., Leu, M., Nakagawa, T., 1998. Progress in additive manufacturing and rapid prototyping. CIRP Ann. – Manuf. Technol. 47 (2), 525–540.

Martinsson, P.-G., Babuška, I., 2007. Mechanics of materials with periodic truss or frame micro-structures. Arch. Ration. Mech. Anal. 185 (2), 201–234.

Messner, M.C., Beaudoin, A.J., Dodds, R.H., 2015. Consistent crystal plasticity kinematics and linearization for the implicit finite element method. Eng. Comput. 32 (6), 1526–1548.

Meza, L.R., Das, S., Greer, J.R., 2014. Strong, lightweight, and recoverable three-dimensional ceramic nanolattices. Science 345 (6202), 1322–1326.

Mohr, D., 2005. Mechanism-based multi-surface plasticity model for ideal truss lattice materials. Int. J. Solids Struct. 42 (11–12), 3235–3260.

Murr, L.E., Gaytan, S.M., Ramirez, D.A., Martinez, E., Hernandez, J., Amato, K.N., Shindo, P.W., Medina, F.R., Wicker, R.B., Jan. 2012. Metal fabrication by additive manufacturing using laser and electron beam melting technologies. J. Mater. Sci. Technol. 28 (1), 1–14.

Nichols, A., 2014. ALE3D User's Manual, Tech. rep., Lawrence Livermore National Laboratory.

Pao, Y.-H., Keh, D.-C., Howard, S.M., 1999. Dynamic response and wave propagation in plane trusses and frames. AIAA J. 37 (5), 594–603.

Rosen, D.W., 2007. Computer-aided design for additive manufacturing of cellular structures. Comput. Aided. Des. Appl. 4 (5), 585–594.

Roters, F., Eisenlohr, P., Hantcherli, L., Tjahjanto, D., Bieler, T., Raabe, D., 2010. Overview of constitutive laws, kinematics, homogenization and multiscale methods in crystal plasticity finite-element modeling: theory, experiments, applications. Acta Mater. 58 (4), 1152–1211.

Schaedler, T.A., Jacobsen, A.J., Torrents, A., Sorensen, A.E., Lian, J., Greer, J.R., Valdevit, L., Carter, W.B., 2011. Ultralight metallic microlattices. Science 334 (6058), 962–965 (80-).

Signorelli, J., von Flotow, A., 1988. Wave propagation, power flow, and resonance in a truss beam. J. Sound Vib. 126 (1), 127–144.

Srikantha Phani, A., Woodhouse, J., Fleck, N.A., 2006. Wave propagation in two-dimensional periodic lattices. J. Acoust. Soc. Am. 119 (4), 1995–2005.

Wang, Z.-P., Sun, C., 2002. Modeling micro-inertia in heterogeneous materials under dynamic loading. Wave Motion 36 (4), 473–485.

Warren, W., Kraynik, A., 1987. Foam mechanics: the linear elastic response of two-dimensional spatially periodic cellular materials. Mech. Mater. 6 (1), 27–37.

Winter, R.E., Cotton, M., Harris, E.J., Maw, J.R., Chapman, D.J., Eakins, D.E., McShane, G., 2014. Plate-impact loading of cellular structures formed by selective laser melting. Model. Simul. Mater. Sci. Eng. 22 (2), 025021.

Yong, Y., Lin, Y., 1992. Dynamic response analysis of truss-type structural networks: a wave propagation approach. J. Sound Vib. 156 (1), 27–45.

Zheng, X., Lee, H., Weisgraber, T.H., Shusteff, M., DeOtte, J., Duoss, E.B., Kuntz, J.D., Biener, M.M., Ge, Q., Jackson, J., Fang, N.X., Spadaccini, C.M., 2014. Ultralight, ultrastiff mechanical metamaterials. Science 344, 1373–1377 (80-.).